scientific reports

Check for updates

OPEN

Stress exposure affects amyotrophic lateral sclerosis pathogenesis via PI3K/Akt and focal adhesion pathways: evidence from three experimental models

Daniela Maria Rasà[1,2], Ilaria Stoppa[1], Noémie Bérenger-Currias[3], Elena Pasho[4], Sorana Ciura[4], Edor Kabashi[4], Cécile Martinat[3] & Marina Boido[1]✉

Amyotrophic lateral sclerosis (ALS) is a multifactorial motor neuron (MN) disease, characterized by several cellular dysfunctions, many of which are shared by different neurodegenerative diseases. Here, we investigated whether a stressful lifestyle might exacerbate the altered mechanisms and affect the disease progression in ALS-predisposed conditions. To model stress in vivo, *SOD1*^{G93A} mice underwent a chronic unpredicted mild stress protocol. This resulted in a significant impairment in body weight gain and motor performance, in a gender-specific manner. Moreover, the gene expression of *Col1a1*, *Col1a2* and *Il6* was strongly dysregulated in motor cortex and/or spinal cord of stressed mice. To assess the direct impact of stress on MNs, NSC-34 h*SOD1*^{G93A} cells underwent oxygen and glucose deprivation. Compared to NSC-34 h*SOD1*^{WT}, mutated MNs exhibited a reduced capacity to cope with stress. By performing gene expression, protein-protein interaction, gene ontology and pathway enrichment analyses, we also revealed the pivotal role of the PI3K/Akt and focal adhesion pathways (triggered by *Gsk3b*, *Il6*, *Igf1* and/or collagen) in mediating stress response. Similar results were observed in stressed human iPSCs-derived *TARDBP*^{G298S} MNs. In conclusion, our results suggest that the PI3K/Akt and focal adhesion pathways play a crucial role in stress response across different ALS-predisposed models: the study paves the way for novel therapeutic targets and highlights the relevance of a healthy lifestyle.

Keywords Bioinformatic analysis, Exposome, Molecular mechanisms, Neuromuscular disease, Stressor

Amyotrophic lateral sclerosis (ALS) is a motor neuron (MN) disease due to the degeneration of upper and lower MNs. The disease is characterized by progressive skeletal muscle weakness and atrophy, until respiratory failure 2–3 years after diagnosis. About 5–10% of patients are affected by the familial form of ALS (fALS), while the remaining 90–95% present a sporadic form (sALS)[1,2]. More than 30 genes have been associated with ALS aetiology, including *SOD1*, *TARDBP*, *FUS* and *C9orf72*, which are responsible for about 60% of fALS cases. Mutations of the same genes are also frequently found in sALS cases[3]. Interestingly, environmental factors can also play a role in the development of the disease[4].

Several molecular mechanisms characterize ALS pathophysiology, including oxidative stress, excitotoxicity, glial dysfunctions, neuroinflammation, mitochondrial alterations, dysregulated nucleocytoplasmic and vesicle transport, impaired protein homeostasis and endoplasmic reticulum stress, axonopathy, impaired DNA damage repair and aberrant RNA metabolism[1].

However, several "stressors", i.e. any kind of physical or psychological disturbance that can affect the optimal functioning of the organism, could also influence ALS pathogenesis, by exacerbating the above-mentioned altered mechanisms[5]. Indeed, the stress response can act on the sympathetic-adreno-medullary axis and hypothalamus-pituitary-adrenal (HPA) axis: the first releases noradrenaline and norepinephrine, while the second secretes glucocorticoids. Both cascades result in short- or long-term consequences throughout the body, including the

[1]Department of Neuroscience "Rita Levi Montalcini", Neuroscience Institute Cavalieri Ottolenghi, University of Turin, Turin, Italy. [2]University School for Advanced Studies IUSS Pavia, Pavia, Italy. [3]Université Paris-Saclay, Université d'Evry, Inserm, I-Stem, UMR861, 91100 Corbeil-Essonnes, France. [4]Laboratory of Translational Research for Neurological Disorders, Imagine Institute, INSERM UMR 1163, 75015, Université Paris Cité, Paris, France. ✉email: marina.boido@unito.it

CNS[6]. Acute stress triggers a rapid response to facilitate and accelerate adaptive responses: the reduction and/or increase in excitatory or inhibitory activity, in specific CNS areas, is modulated to restore physiological balance and increase resilience[6,7]. However, a prolonged exposure to stressful events, typical of chronic stress, increases ROS, triggers neuroinflammation and cell death, alters cellular morphology and decreases axon activity[8].

Unfortunately, stress is increasing in our modern society due to the global and lifestyle changes, potentially affecting the onset and progression of neurodegenerative diseases in particular in predisposed individuals, while healthy habits could counteract the acceleration of these pathologies[9,10]. In this regard, the present study aimed to investigate the stress impact on ALS pathogenesis and to identify the specific molecular mechanisms and genes involved. We used both in vivo and in vitro models: first, the stress effects were evaluated in vivo using h*SOD1*^{G93A} mice to investigate the expression of several ALS-related genes in both motor cortex and lumbar spinal cord. Then, to specifically study the stress effect on MNs, we used murine h*SOD1*^{G93A} NSC-34 cell lines and human *TARDBP*^{G298S} iPSCs-derived MNs, which underwent oxygen-glucose deprivation (OGD), with the aim to further explore stress-affected genes and molecular pathways.

Results

In vivo study of stress effects in female and male h*SOD1*^{G93A} mice

To verify whether stress could affect disease progression in ALS-predisposed conditions, its effect was evaluated in h*SOD1*^{G93A} mice. To this end, mice were subjected to a 28-day chronic unpredicted mild stress protocol[11,12], followed by behavioural observations and molecular analyses (RT-qPCR) (Fig. 1; Fig. S1).

Concerning the females, the rotarod performance was significantly reduced at the end of the stress period (end point) compared to the beginning (starting point), whereas no differences were observed in males (Fig. 1A and C). Body weight remained unchanged after the 28 day-stress protocol, in both female and male ALS stressed

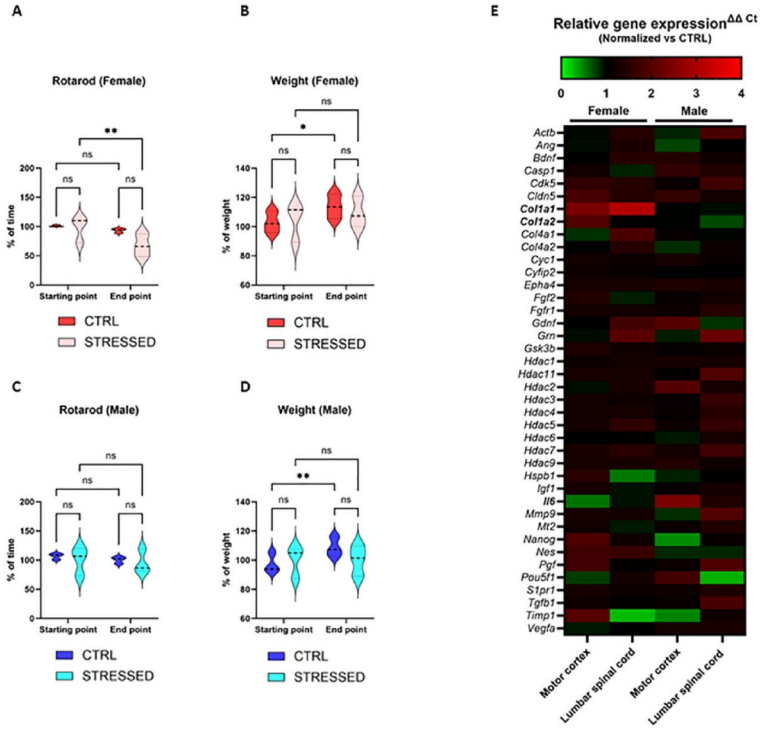

Fig. 1. Chronic unpredicted mild stress effects in female and male ALS-predisposed mice. A-B. Rotarod and weight results in female h*SOD1*^{G93A} are showed at starting and end point in STRESSED and CTRL (not stressed) groups. Results are represented as median and quartile range of three mice per group, considering the average of three trials. Mixed-effects analysis followed by Uncorrected Fisher's LDS analysis was used for statistical results. Rotarod of female h*SOD1*^{G93A} STRESSED at end point vs. female h*SOD1*^{G93A} STRESSED at starting point $^{**}p < 0.01$; weight of female h*SOD1*^{G93A} CTRL at end point vs. female h*SOD1*^{G93A} CTRL at starting point $^{*}p < 0.05$. C-D. Rotarod and weight results in male h*SOD1*^{G93A} are described at starting and end point in STRESSED and CTRL (not stressed) groups. Results are represented as median and quartile range of three mice per groups, considering the average of three trials. Mixed-effects analysis followed by Uncorrected Fisher's LDS analysis was used for statistical results. Weight of male h*SOD1*^{G93A} CTRL at end point vs. male h*SOD1*^{G93A} CTRL at starting point $^{**}p < 0.01$. E. Heatmap graph (created using GraphPad Prism version 10.1.2 for Windows) shows the relative gene expression in motor cortex and lumbar spinal cord samples of STRESSED groups normalized to CTRL (distinguishing female and male groups). Results are showed as red-to-green scale, using data of three mice per groups and indicating 1 (black) as baseline reference point of female or male h*SOD1*^{G93A} CTRL (not shown). Two-way ANOVA followed by Sidák's multiple comparison test was used as statistical analysis and the significantly results were listed in Table 1.

mice (Fig. 1B and D). In contrast, it was significantly increased in absence of stress, as expected for young growing mice.

Regarding the RT-qPCR analysis, the relative gene expression of 39 ALS-correlated genes (see gene list in Table S1; Prime PCR Disease State Panels, Bio-Rad Laboratories) was investigated in both motor cortex and lumbar spinal cord samples, by normalizing the values of stressed h*SOD1*^{G93A} mice (STRESSED) to not-stressed h*SOD1*^{G93A} mice (CTRL) (Fig. 1E). As summarized in Table 1, *Col1a1* was significantly up-regulated in stressed females as compared to CTRL ones, both in the motor cortex and lumbar spinal cord. *Col1a2* was also up-regulated in the female group, but only in the motor cortex. Instead, *Il6* was significantly up-regulated in stressed ALS male mice compared to CTRL ones in the motor cortex, whereas no statistically significant differences in the expression of other genes were observed in lumbar spinal cord samples.

Characterization of NSC-34 differentiation in MN-like cells

To investigate the direct effect of stress on ALS MNs, we first used NSC-34 MN-like cells, a hybrid cell line derived by spinal cords of mouse embryos and mouse neuroblastoma cells.

First, we defined the cell differentiation conditions. Differentiation of NSC-34 cells (naïve, h*SOD1*^{WT} and h*SOD1*^{G93A}) into MN-like cells was obtained by using serum starvation and RA treatment: various RA concentrations were tested at different DIV (Days In Vitro) by the MTT assay to identify the highest non-toxic concentration that did not interfere with the doxycycline effect (needed for the h*SOD1* gene activation). By testing different RA concentrations (namely 1, 5, 10, 15 and 20 µM) and normalizing data to naïve NSC-34 cells, the cell viability of h*SOD1*^{G93A} cells was significantly different compared to the h*SOD1*^{WT} ones, almost at each DIV (Fig. S2). However, by analysing each cell type independently (Fig. S3), we identified a 4 day-RA treatment as the optimal condition to obtain MN-like cell differentiation in each condition, in agreement with the literature[13]: in fact cell viability was unchanged at DIV4 in all cell lines, w/wo doxycycline, using any RA concentration as compared to control condition (1% serum) (Fig. S3A-F). On the contrary, cell viability at DIV2, 6 and 8 was significantly modified with almost all the RA concentrations.

Then, the following morphological analyses were performed for all NSC-34 cell lines combining serum starvation (1% serum) with 20 µM of RA for 4 DIV (i.e. the highest non-toxic concentration at 4 DIV), in order to assess the MN differentiation. As shown in Fig. 2, in presence of RA, cell-body clusters, neurite length and branching were significantly increased in NSC-34 naïve (Fig. 2A-D), h*SOD1*^{WT} (Fig. 2E-H) and h*SOD1*^{G93A} (Fig. 2I-L), w/wo doxycycline, as compared to control conditions (1% serum w/o RA). The MN maturation was demonstrated by analysing ChAT expression by immunofluorescence (IF): by culturing cells in 1% serum and RA 20 µM, w/wo doxycycline, the corrected total cell fluorescence (CTCF) was significantly increased in NSC-34 naïve (Fig. 2M-N), h*SOD1*^{WT} (Fig. 2O-P) and h*SOD1*^{G93A} (Fig. 2Q-R), compared to control cells (1% serum only). No significant differences in morphological parameters, nor in ChAT expression have been observed among the cell lines, upon doxycycline administration (Fig. S4). These results confirm that all NSC-34 lines underwent proper differentiation into MN-like cells, supporting the conclusion that any subsequent differences observed could not be due to variability in the differentiation process.

Until this point, naïve cells were included to validate the cell differentiation protocol and exclude potential interferences between the RA administration and the doxycycline treatment, and vice versa. However, from this point onward forward, we have excluded naïve cells to avoid inappropriate comparisons between different experimental systems: indeed h*SOD1* NSC-34 cells express a hemagglutinin's epitope, making them a modified system. Thus, h*SOD1*^{WT} will be considered the most appropriate control for the following analyses and statistical comparisons.

Oxygen-glucose deprivation (OGD) as a stress model in vitro

OGD was used to model a chronic stress in vitro. We evaluated different concentrations of $CoCl_2$ (a hypoxia-mimetic agent) in low glucose medium for 24 h, using the MTT assay to determine the dose inducing approximatively 50% cell death. As shown in Fig. 3A, all the employed $CoCl_2$ concentrations (50, 100, 200, 300 and 400 µM) significantly reduced cell viability in both NSC-34 h*SOD1*^{WT} and h*SOD1*^{G93A} cells, as compared to low glucose condition. However, 100 µM $CoCl_2$ was the lowest concentration that induced 50% cell loss and revealed a significant difference between NSC-34 h*SOD1*^{WT} and h*SOD1*^{G93A} (Fig. 3A). Therefore, this concentration was used in subsequent experiments, starting with the OGD stress effect validation.

First, we evaluated the mitochondrial potential membrane status in NSC-34 h*SOD1*^{WT} and h*SOD1*^{G93A} cells, both in stressed and not-stressed (CTRL) conditions. We analysed the integrated intensity normalized to phase object count using MitoTracker Red CMXRos (Fig. 3B-C). The signal intensity showed only a decreasing trend in h*SOD1*^{WT} stressed cells respect to CTRL, while it was significantly reduced in h*SOD1*^{G93A} stressed cells as

Gene	Comparison	Tissue	Sex	*p*-value
Col1a1	STRESSED vs. CTRL	Motor cortex	Female	0.0021
Col1a2	STRESSED vs. CTRL	Motor cortex	Female	0.0055
Col1a1	STRESSED vs. CTRL	Spinal cord	Female	< 0.0001
Il6	STRESSED vs. CTRL	Motor cortex	Male	< 0.0001

Table 1. Genes significantly deregulated in Fig. 1. Significant statistically differences referred to relative gene expression ($2^{-\Delta\Delta Ct}$ method) of hSOD1^{G93A} stressed (STRESSED) mice normalized to h*SOD1*^{G93A} non-stressed (CTRL) mice per each tissue. Two-way ANOVA was applied as statistical analysis.

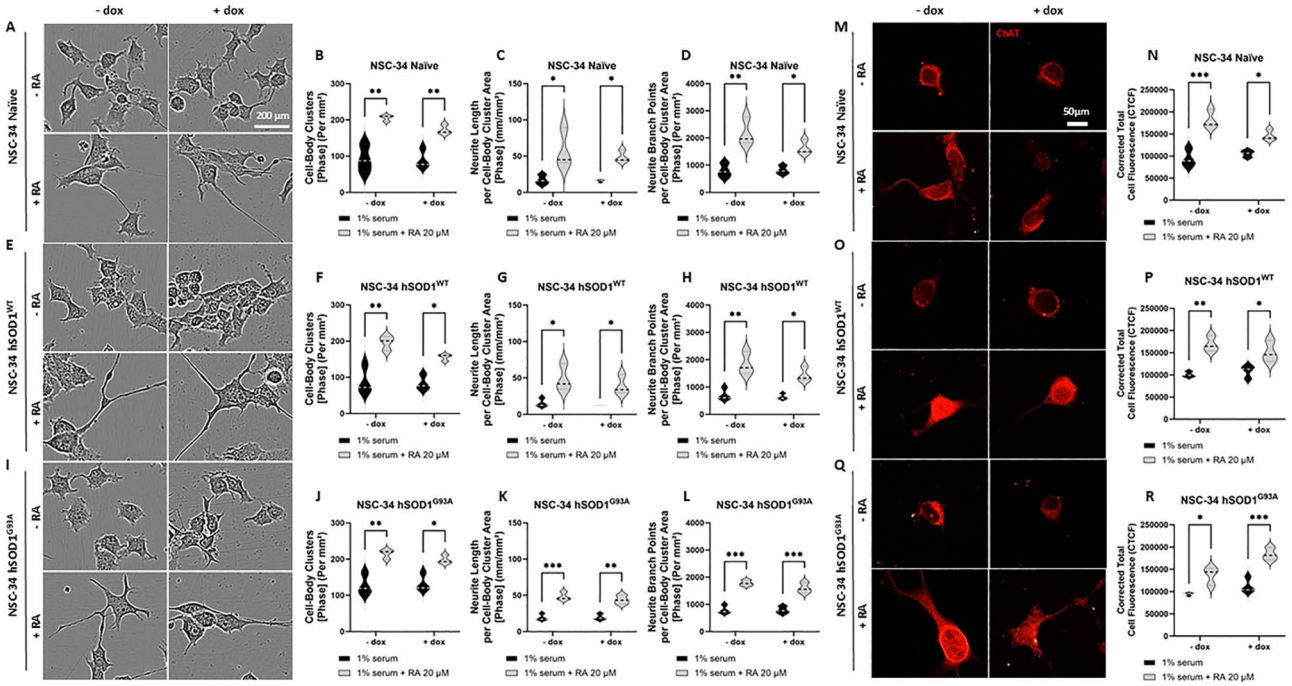

Fig. 2. Morphological analysis related to RA treatment (20 µM for 4 days). A, E, I. Representative images acquired using the built-in Basler Ace 1920 –155 µm camera of the Incucyte system. Scale bar = 200 µm. B-D, F-H, J-L. Cell-body cluster, neurite length and neurite branch point are significantly increased after RA treatment, w/wo doxycycline in NSC-34 naïve, h*SOD1*^{WT} and h*SOD1*^{G93A}. Results are represented as median and quartile range of three independent experiments. Two-way ANOVA followed by Sidák's multiple comparisons test was used as statistical analysis. 1% serum + RA 20 µM vs. 1% serum $^{*}p < 0.05$, $^{**}p < 0.01$ and $^{***}<0.001$. M, O, Q. NSC-34 naïve, h*SOD1*^{WT} h*SOD1*^{G93A} treated with RA and immunolabeled by anti-ChAT antibody (red). Representative images acquired by Eclipse E600 (Microfire Camera 2-Megapixel Color Imaging, 1600 × 1200). Scale bar = 50 µm. N, P, R. CTCF is significantly increased in NSC-34 naïve, h*SOD1*^{WT} h*SOD1*^{G93A}, w/wo doxycycline. Results are represented as median and quartile range of three independent experiments ($n \geq 10$ neurons for each experiment). Two-way ANOVA followed by Sidák's multiple comparisons test was used as statistical analysis. 1% serum + RA 20 µM vs. 1% serum $^{*}p < 0.05$, $^{**}p < 0.01$ and $^{***}<0.001$.

compared to CTRL conditions. Even if stress exposure elicited a comparable response trend in both cell lines, it induced significant changes only in h*SOD1*^{G93A} cells, highlighting a possible mitochondrial impairment and an increased vulnerability only in stressed NSC-34 h*SOD1*^{G93A} cells. These findings suggest a cumulative effect of the *SOD1*^{G93A} mutation and cellular stress.

To further validate this effect, the expression of specific hypoxic (HIF1α) and pro-apoptotic (cleaved caspase 3) markers was investigated by western blot (Fig. 3D-F; Fig. S5). The HIF1α protein levels were significantly up-regulated under stress conditions in h*SOD1*^{WT} cells, while no remarkable differences were observed in h*SOD1*^{G93A} cells (possibly due to their already impaired state). Interestingly, a significant down-regulation was observed in stressed h*SOD1*^{G93A} compared to stressed h*SOD1*^{WT} cells (Fig. 3E). Similarly, a significant up-regulation of cleaved caspase 3 protein levels was noted in h*SOD1*^{WT} cells after stress exposure compared to CTRL condition (Fig. 3F). In h*SOD1*^{G93A} cells the stress apparently did not induce remarkable effects: cleaved caspase 3 protein levels were significantly increased in not-stressed h*SOD1*^{G93A} cells compared to h*SOD1*^{WT} ones (Fig. 3F). Overall, these results highlight a reduced ability of h*SOD1*^{G93A} to endure and respond to stress conditions, also denoting the activation of cell death pathways in CTRL conditions.

Gene expression analysis in NSC-34 h*SOD1* upon stress exposure

Once validated the OGD stress model, the expression of the 39 ALS-correlated genes was analysed by RT-qPCR in NSC-34 h*SOD1*^{WT} and h*SOD1*^{G93A} in basal conditions (CTRL) or upon stress exposure (STRESSED). As shown in the heatmap of Fig. 4A, most of the genes were deregulated under stress conditions, both in WT and mutated cells, in comparison to NSC-34 h*SOD1*^{WT} CTRL. Seventeen out of 39 genes were found to be significantly deregulated (the statistical details are listed in Table 2) and included: *Ang*, *Bdnf*, *Casp1*, *Cldn5*, *Col1a1*, *Col4a1*, *Col4a2*, *Fgfr1*, *Gsk3b*, *Hdac7*, *Hspb1*, *Igf1*, *Il6*, *Nanog*, *Nes*, *Pou5f1* and *Tfgb1*.

To understand whether these specific deregulations were mutation-dependent, i.e. disease-related, and/or triggered by stress in disease-predisposed conditions, the expression level of these 17 genes was analysed by comparing h*SOD1*^{G93A} CTRL vs. h*SOD1*^{WT} CTRL MNs and, independently, h*SOD1*^{G93A} STRESSED vs. h*SOD1*^{WT} STRESSED MNs (Fig. 4B). These analyses revealed the significant deregulation of 11 and 10 genes in h*SOD1*^{G93A} versus to h*SOD1*^{WT} MNs in CTRL (Fig. 4C) and STRESSED condition, respectively (Fig. 4D). As

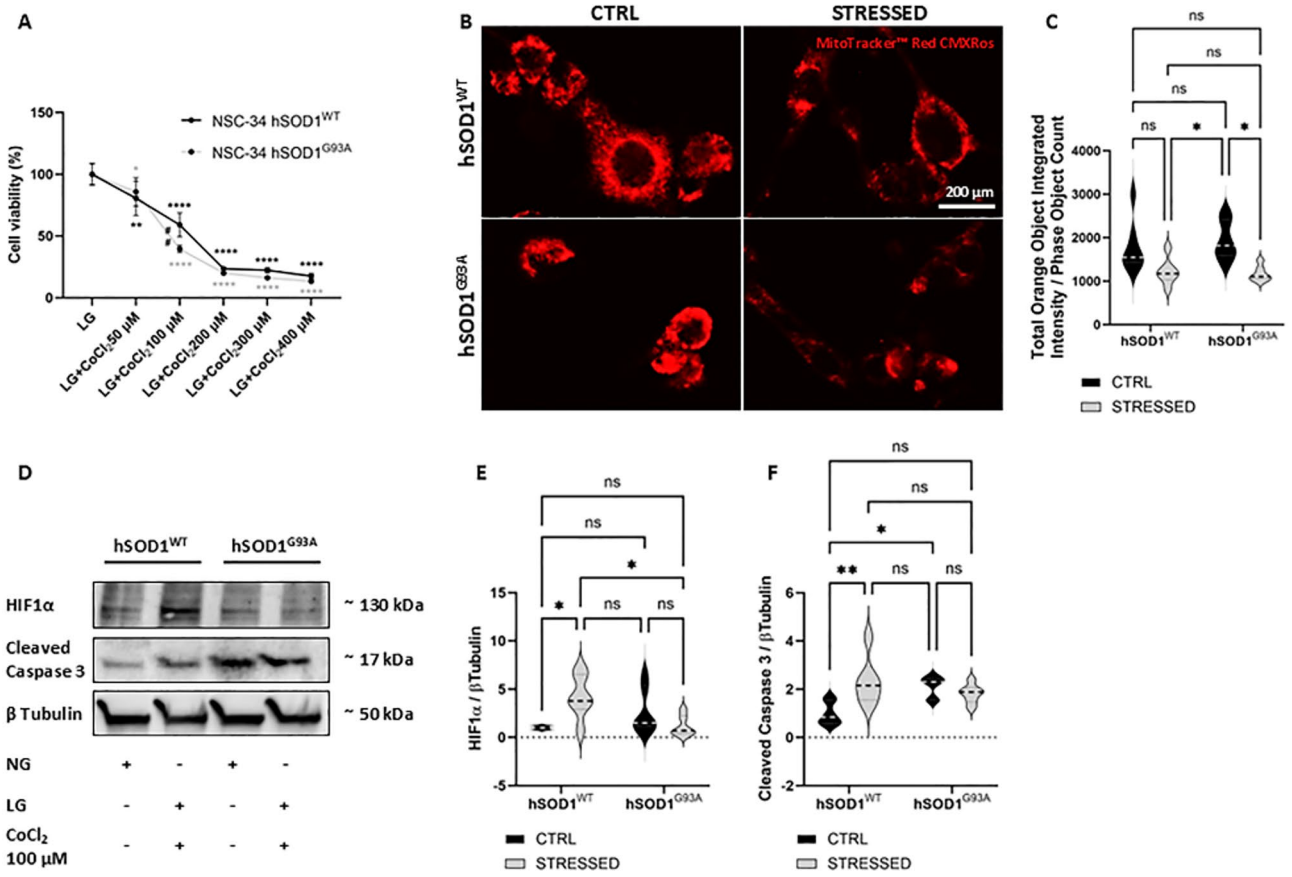

Fig. 3. OGD stress validation in NSC-34 h*SOD1* cells. (A) The in vitro stress model was established using OGD conditions, by culturing NSC-34 cells in low glucose (LG) medium and $CoCl_2$. All the tested concentrations of $CoCl_2$ (50, 100, 200, 300 and 400 µM) are able to induce a reduction of cell viability, both in NSC-34 h$SOD1^{WT}$ and h$SOD1^{G93A}$, compared to LG culture; ~50% of cell death is observed using 100 µM of $CoCl_2$. Results are represented as mean ± SD of three independent experiments. Two-way ANOVA followed by Sidák's multiple comparisons test was used for comparing different LG and $CoCl_2$ concentrations in each cell line and different cell lines in each experimental condition. LG + $CoCl_2$ 50 µM/ 100 µM/ 200 µM/ 300 µM/ 400 µM vs. LG $^*p < 0.05$, $^{**}p < 0.01$ and $^{****}p < 0.0001$. NSC-34 h$SOD1^{G93A}$ vs. NSC-34 h$SOD1^{WT}$ $^{\#}p < 0.01$. (B) NSC-34 h$SOD1^{WT}$ and h$SOD1^{G93A}$, CTRL or STRESSED, were treated with MitoTracker Red CMXRos. Representative images acquired in live imaging by built-in Basler Ace 1920 –155 µm camera of the Incucyte system. (C) Quantifications of orange signal (visible in red), related to mitochondria membrane potential, performed using automated fluorescent analysis of the Incucyte system. Total orange object integrated intensity results is normalized to phase object count. Results are represented as median and quartile range of six independent experiments. Two-way ANOVA followed by Tukey's multiple comparison test was used as statistical analysis. NSC-34 h$SOD1^{G93A}$ CTRL vs. NSC-34 h$SOD1^{WT}$ STRESSED and NSC-34 h$SOD1^{G93A}$ STRESSED vs. NSC-34 h$SOD1^{G93A}$ CTRL $^*p < 0.05$. (D) Representative images showing HIF1α and cleaved caspase 3 protein levels of NSC-34 h$SOD1^{WT}$ and h$SOD1^{G93A}$, in both experimental conditions (CTRL and STRESSED). NG stands for Normal Glucose. E-F. Protein expression levels quantified by normalizing all experimental conditions vs. NSC-34 h$SOD1^{WT}$ CTRL. Full-length blots are shown in Fig. S5. Results are represented as median and quartile range of three independent experiments. Two-way ANOVA followed by Tukey's multiple comparison test was used as statistical analysis. NSC-34 h$SOD1^{WT}$ STRESSED vs. NSC-34 h$SOD1^{WT}$ CTRL $^*p < 0.05$ and $^{**}p < 0.01$; h$SOD1^{G93A}$ STRESSED vs. NSC-34 h$SOD1^{WT}$ STRESSED $^*p < 0.05$; h$SOD1^{G93A}$ CTRL vs. NSC-34 h$SOD1^{WT}$ CTRL$^*p < 0.05$.

shown in Fig. 4C, *Cldn5* was significantly down-regulated, while *Bdnf*, *Casp1*, *Col4a1*, *Fgfr1*, *Gsk3b*, *Hdac7*, *Igf1*, *Il6*, *Nanog* and *Tgfb1* were up-regulated in h$SOD1^{G93A}$ CTRL cells compared to h$SOD1^{WT}$ CTRL. These findings indicate that the expression of these genes is significantly modulated by the presence of the mutation itself.

Instead, upon stress exposure, *Ang*, *Cldn5*, *Gsk3b*, *Hdac7*, Hspb1, *Il6* were significantly down-regulated (Table 2) in ALS mutated MNs compared to h$SOD1^{WT}$ cells, whereas *Casp1*, *Col4a2*, *Igf1* and *Tgfb1* were significantly up-regulated (Fig. 4D). Therefore, the stress exposure can affect the expression of some genes in h$SOD1^{G93A}$ STRESSED cells.

To predict the interactions among the proteins synthetized by the deregulated genes of interest, we evaluated CTRL and STRESSED conditions through separated protein-protein interaction (PPI) networks by STRING

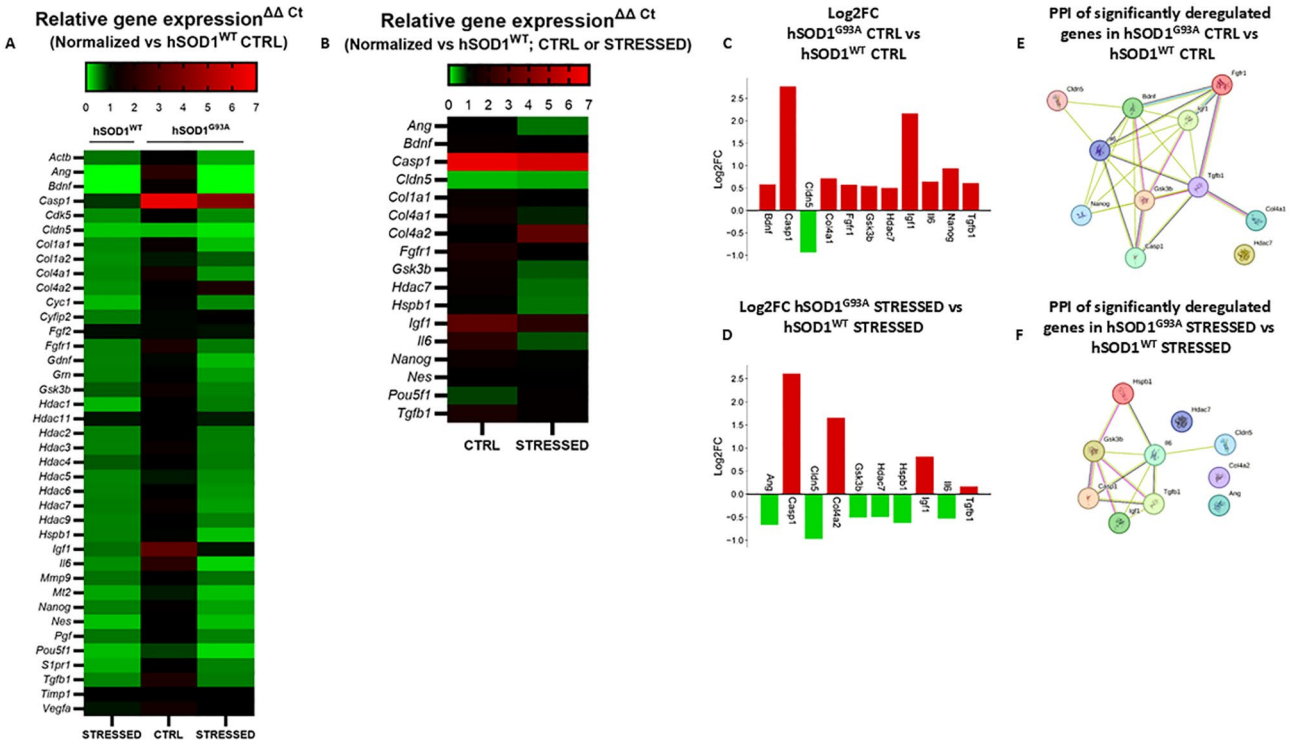

Fig. 4. Gene expression and relative PPI in CTRL and STRESSED cells. (A) Heatmap graph (created using GraphPad Prism version 10.1.2 for Windows) shows relative gene expression of NSC-34 h*SOD1*^{WT} STRESSED, NSC-34 h*SOD1*^{G93A} CTRL and STRESSED, normalized to NSC-34 h*SOD1*^{WT} CTRL. Results are showed as red-to-green scale of nine independent experiments, indicating 1 (black) as baseline of NSC-34 h*SOD1*^{WT} CTRL (not shown). Two-way ANOVA followed by Tukey's multiple comparisons test was used as statistical analysis and the details were listed in Table 2. (B) Heatmap graph (created using GraphPad Prism version 10.1.2 for Windows) shows the relative expression of genes of interest, in both CTRL and STRESSED experimental conditions. Results are showed as red-to-green scale of nine independent experiments, indicating 1 (black) as baseline of NSC-34 h*SOD1*^{WT} (not shown). Unpaired t-test statistical analysis for each gene was used: NSC-34 h*SOD1*^{G93A} CTRL vs. NSC-34 h*SOD1*^{WT} CTRL, NSC-34 h*SOD1*^{G93A} STRESSED vs. NSC-34 h*SOD1*^{WT} STRESSED. C-D. Bar plot graphs show the genes significantly up-regulated and/or down-regulated, based on the unpaired t-test statistical analysis previously described in CTRL and STRESSED conditions. E-F. PPI, performed by STRING analysis, shows interactions among predicted proteins in CTRL and STRESSED conditions.

analysis (Fig. 4E-F). All the proteins, excluding *Hdac7*, were predicted to interact among each other in CTRL condition (Fig. 4E); while, the PPIs were reduced upon stress exposure: in particular *Ang*, *Col4a2* and *Hdac7* did not show any interaction with the other predicted proteins (Fig. 4F).

Gene ontology (GO) and pathway enrichment analysis were performed on genes previously described in the bar plots of Fig. 4C-D for both experimental conditions. As shown in Fig. 5A and C, biological processes (BP), cellular components (CC) and molecular function (MF) revealed some similarities between the two groups (i.e. CTRL and STRESSED). However, among the BPs, "*positive regulation of protein transport*", "*positive regulation of establishment of protein localization*", "*positive regulation of protein secretion*", "*positive regulation of peptide secretion*", and "*regulation of interleukin-1 beta production*" were detected only upon stress exposure. Similarly, a limited numbers of CCs and MFs were specific for STRESSED experimental conditions: "*basement membrane*", "*grow cone*", "*site of polarized growth*" (in the framework of CCs) and "*protein kinase regulator activity*", "*kinase regulator activity*", "*protein kinase C binding*" (referred to MFs). Finally, pathway enrichment analysis identified "*PI3K-Akt signalling pathway*" as a relevant pathway in both CTRL and STRESSED conditions, while "*Focal adhesion*" as implicated only in STRESSED one (Fig. 5B and D). Although PI3K-Akt signalling pathway was relevant into both analyses, the genes were involved in different manner: by comparing STRESSED and CTRL conditions, we observed that (i) *Gsk3b* and *Il6* were differentially deregulated, (ii) two *Col4* chains were implicated (*Col4a1* in CTRL analysis and *Col4a2* in STRESSED analysis), (iii) only *Igf1* was up-regulated in both cases. In addition, *Fgfr1* and *Bdnf* were involved only in CTRL condition. Interestingly, *Gsk3b*, *Igf1* and *Col4a2* were also implicated in the "*Focal adhesion*", the specific mechanism related to STRESSED analysis.

Investigation of stress effects in ALS *TARDBP*^{G298S} human iPSC-derived MNs

In order to extend these analyses to human cells, the same OGD stress was applied to hiPSC-derived MNs, either healthy (56c2) or bearing the TDP43 mutation - *TARDBP*^{G298S} - (Fig. 6A). Interestingly, TARDBP

Gene	Comparison	*p*-value
Ang	h*SOD1*^{WT} STRESSED vs. h*SOD1*^{WT} CTRL	0.0055
	h*SOD1*^{G93A} CTRL vs. h*SOD1*^{WT} CTRL	< 0.0001
	h*SOD1*^{G93A} STRESSED vs. h*SOD1*^{WT} CTRL	0.0055
	h*SOD1*^{G93A} CTRL vs. h*SOD1*^{WT} STRESSED	< 0.0001
	h*SOD1*^{G93A} STRESSED vs. h*SOD1*^{G93A} CTRL	< 0.0001
Bdnf	h*SOD1*^{WT} STRESSED vs. h*SOD1*^{WT} CTRL	0.0155
	h*SOD1*^{G93A} STRESSED vs. h*SOD1*^{WT} CTRL	0.0079
	h*SOD1*^{G93A} CTRL vs. h*SOD1*^{WT} STRESSED	< 0.0001
	h*SOD1*^{G93A} STRESSED vs. h*SOD1*^{G93A} CTRL	< 0.0001
Casp1	h*SOD1*^{G93A} CTRL vs. h*SOD1*^{WT} CTRL	< 0.0001
	h*SOD1*^{G93A} STRESSED vs. h*SOD1*^{WT} CTRL	< 0.0001
	h*SOD1*^{G93A} CTRL vs. h*SOD1*^{WT} STRESSED	< 0.0001
	h*SOD1*^{G93A} STRESSED vs. h*SOD1*^{WT} STRESSED	< 0.0001
	h*SOD1*^{G93A} STRESSED vs. h*SOD1*^{G93A} CTRL	< 0.0001
Cldn5	h*SOD1*^{WT} STRESSED vs. h*SOD1*^{WT} CTRL	0.0424
	h*SOD1*^{G93A} STRESSED vs. h*SOD1*^{WT} CTRL	0.0108
Col1a1	h*SOD1*^{G93A} CTRL vs. h*SOD1*^{WT} STRESSED	0.0308
	h*SOD1*^{G93A} STRESSED vs. h*SOD1*^{G93A} CTRL	0.0073
Col4a1	h*SOD1*^{G93A} CTRL vs. h*SOD1*^{WT} STRESSED	< 0.0001
	h*SOD1*^{G93A} STRESSED vs. h*SOD1*^{G93A} CTRL	0.0002
Col4a2	h*SOD1*^{G93A} STRESSED vs. h*SOD1*^{WT} STRESSED	0.0139
Fgfr1	h*SOD1*^{G93A} CTRL vs. h*SOD1*^{WT} STRESSED	0.0042
	h*SOD1*^{G93A} STRESSED vs. h*SOD1*^{G93A} CTRL	0.0183
Gsk3b	h*SOD1*^{G93A} CTRL vs. h*SOD1*^{WT} STRESSED	0.0396
	h*SOD1*^{G93A} STRESSED vs. h*SOD1*^{G93A} CTRL	0.0032
Hdac7	h*SOD1*^{G93A} CTRL vs. h*SOD1*^{WT} STRESSED	0.0123
	h*SOD1*^{G93A} STRESSED vs. h*SOD1*^{G93A} CTRL	0.0048
Hspb1	h*SOD1*^{G93A} STRESSED vs. h*SOD1*^{G93A} CTRL	0.0349
Igf1	h*SOD1*^{G93A} CTRL vs. h*SOD1*^{WT} CTRL	< 0.0001
	h*SOD1*^{G93A} CTRL vs. h*SOD1*^{WT} STRESSED	< 0.0001
	h*SOD1*^{G93A} STRESSED vs. h*SOD1*^{G93A} CTRL	< 0.0001
Il6	h*SOD1*^{WT} STRESSED vs. h*SOD1*^{WT} CTRL	0.0906
	h*SOD1*^{G93A} STRESSED vs. h*SOD1*^{WT} CTRL	0.0236
	h*SOD1*^{G93A} CTRL vs. h*SOD1*^{WT} STRESSED	0.0001
	h*SOD1*^{G93A} STRESSED vs. h*SOD1*^{G93A} CTRL	< 0.0001
Nanog	h*SOD1*^{G93A} CTRL vs. h*SOD1*^{WT} STRESSED	0.0001
	h*SOD1*^{G93A} STRESSED vs. h*SOD1*^{G93A} CTRL	< 0.0001
Nes	h*SOD1*^{G93A} STRESSED vs. h*SOD1*^{WT} CTRL	0.0430
Pou5f	h*SOD1*^{WT} STRESSED vs. h*SOD1*^{WT} CTRL	0.0458
	h*SOD1*^{G93A} STRESSED vs. h*SOD1*^{WT} CTRL	0.0299
Tgfb1	h*SOD1*^{G93A} CTRL vs. h*SOD1*^{WT} STRESSED	0.0026
	h*SOD1*^{G93A} STRESSED vs. h*SOD1*^{G93A} CTRL	0.0012

Table 2. Genes significantly deregulated in Fig. 4. Significant statistically differences referred to relative gene expression ($2^{-\Delta\Delta Ct}$ method) and normalized to NSC-34 h*SOD1*^{WT} CTRL. Two-way ANOVA was applied as statistical analysis.

mutations are more prevalent than SOD1 mutations: therefore, the use of TARDBP mutated cells may support the generalizability of our findings across distinct ALS subtypes.

We observed that the neurite length (Fig. 6B) and branch points (Fig. 6C) were significantly reduced in TDP-43 MNs as compared to the healthy ones in basal conditions. Upon stress exposure, all the morphological parameters were remarkably changed in healthy cells compared to not stressed condition (CTRL). No significant differences were observed in TDP-43 mutated iPSC-derived MNs upon stress exposure, as compared to CTRL ones. Notably, all the morphometric parameters were significantly affected in mutated cells (both CTRL and STRESSED), compared to healthy MNs CTRL (Fig. 6B-C), emphasizing that the morphological alterations affecting TDP-43 cells are already evident in basal conditions.

Regarding the molecular aspects, we investigated the expression of the genes previously identified in the murine MN analysis, by normalizing healthy STRESSED, TDP-43 CTRL and TDP-43 STRESSED MNs vs.

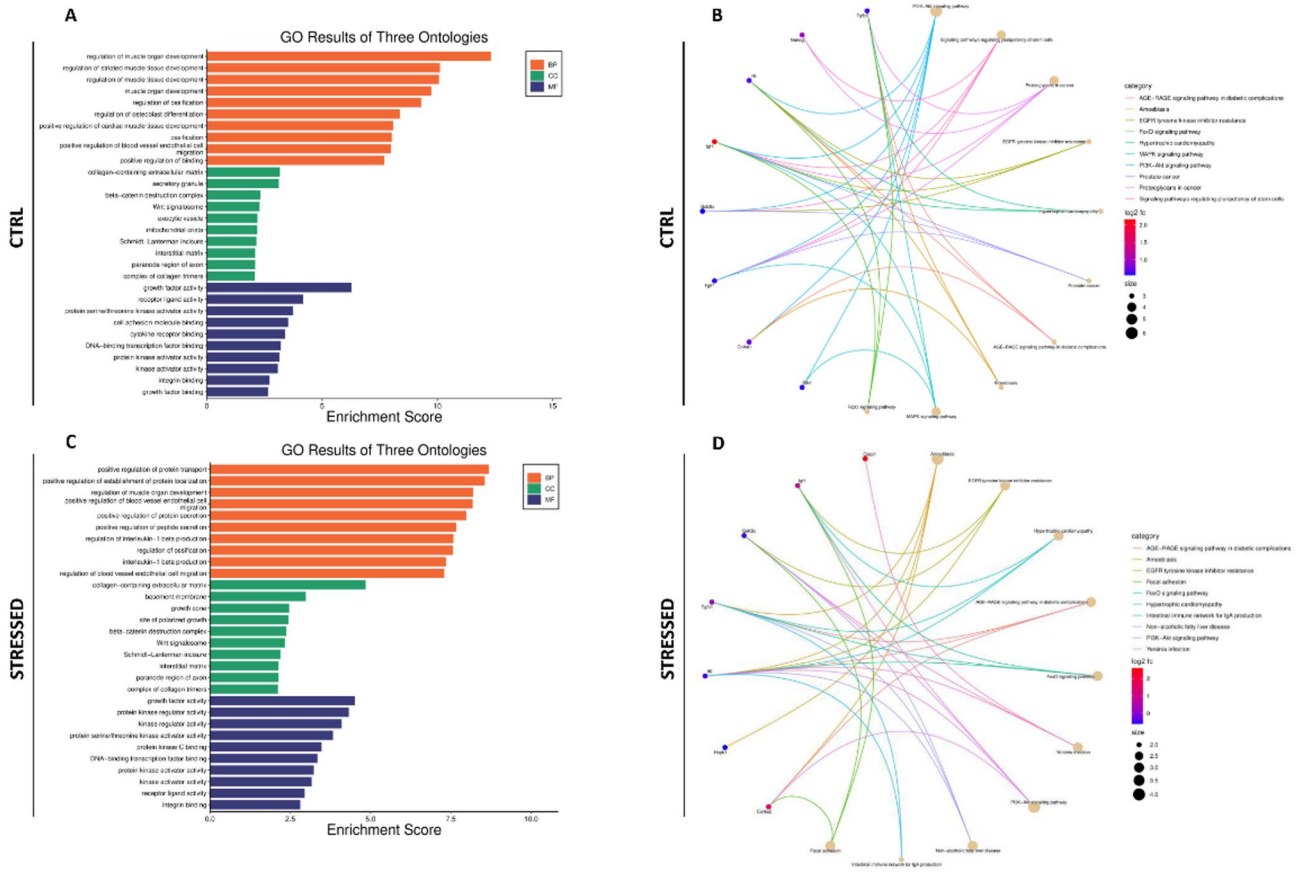

Fig. 5. GO and pathway enrichment analysis in CTRL and STRESSED NSC-34 cells. A-B. Log2FC of gene expression related to NSC-34 h*SOD1*^{G93A} and NSC-34 h*SOD1*^{WT} for CTRL condition, was used to performed GO (including BP, CC and MF in GO three ontology plots) and pathway enrichment analysis by SRplot (free online platform: http://www.bioinformatics.com.cn/SRplot, accessed on 8 May 2024).C-D Log2fc of interesting gene expression related to NSC-34 h*SOD1*^{G93A} and NSC-34 h*SOD1*^{WT} for STRESSED condition, was used to performed GO (including BP, CC and MF in GO three ontology plots) and pathway enrichment analysis by SRplot (free online platform: http://www.bioinformatics.com.cn/SRplot, accessed on 15 March 2024).

healthy CTRL MNs. Similarly to h*SOD1* mouse cells, despite the different mutation, the majority of the selected genes (in particular *Ang*, *Col1a1*, *Col1a2*, *Col4a1*, *Col4a2*, *Hdac7*, *Igf1*) were significantly up-regulated in mutated hiPSC-derived MNs compared to healthy ones under CTRL conditions (Fig. 6D-M). Moreover, following stress exposure, nearly all analyzed genes (except *Casp1* and *Il6*) were significantly down-regulated in TDP-43 MNs compared to mutated CTRL MNs. On the other hand, upon stress exposure, few selected genes, including *Ang*, *Col1a1* and *Col4a2* were significantly up-regulated in TDP-43 MNs compared to healthy ones, while only *Gsk3b* was significantly down-regulated (Fig. 6D-M). Overall, these findings highlight once again the key role of *Gsk3b*, confirming the previous observations in the NSC-34 cells.

Discussion

Our lifestyle can positively or negatively affect our health. Among various factors, the importance of regular physical activity, a balanced diet and adequate sleep has been widely studied, and it is well recognized that these elements can greatly influence our overall wellbeing[14]. In contrast, harmful life habits or specific events can induce stress, potentially contributing to the development of dementia, AD and PD[10,15–17]. Additionally, post-traumatic stress disorders have been identified as risk factors for the onset of PD[10,18,19] and frontotemporal dementia[20]. However, the precise link between a stressful lifestyle and ALS pathogenesis remains unclear. An international online case-control study found no association between stressors and ALS[21], while a Japanese case-control study suggested that a combination of different lifestyle factors, along with reduced antioxidant defences in MNs, may increase ALS risk[22]. In our study, we aimed to clarify the potential relationship between stress and ALS pathogenesis, by exploring the molecular mechanisms triggered by stress in ALS-predisposed conditions, using both in vivo (*SOD1*^{G93A} mice) and in vitro (h*SOD1*^{G93A} NSC-34 and TDP43-mutated hiPSC-derived MNs) models.

First, we employed the most largely known ALS mouse model, the *SOD1*^{G93A} mice, to conduct a pilot study assessing whether stress exposure could affect the disease onset and progression (Fig. 1; Fig. S1). Due to the well-recognized gender ALS-related differences, we considered females and males separately. We mimicked a

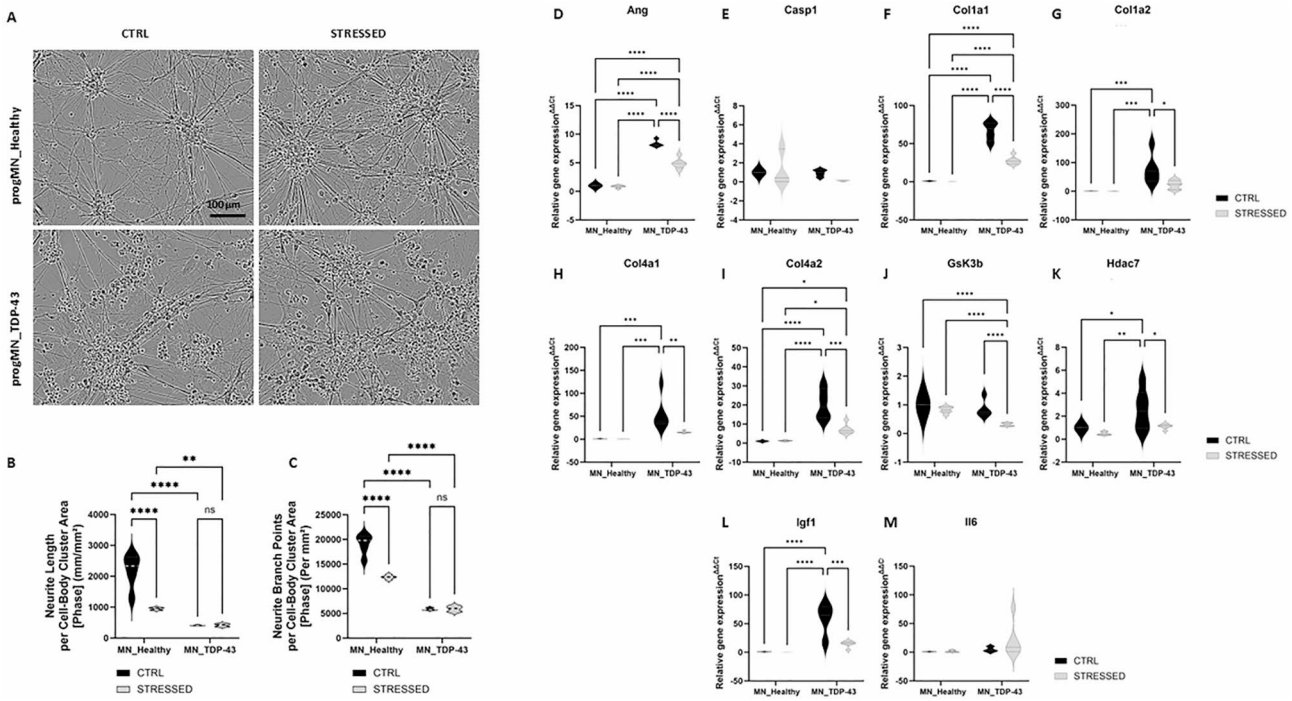

Fig. 6. OGD stress effects in human MNs (healthy and TDP-34). A. Representative images acquired using the built-in Basler Ace 1920 –155 µm camera of the Incucyte system. Scale bar = 100 µm. B-C. Neurite length and branch points are significantly changed upon stress exposure in healthy MNs (MN_healthy). TDP-43 MNs (MN_TDP-43) show relevant morphological alterations both in not stressed (CTRL) and STRESSED experimental conditions, as compared to healthy cells. Results are represented as median and quartile range of three independent experiments. Two-way ANOVA followed by Uncorrected Fisher's LSD analysis was used for statistical results. MN_healthy STRESSED, MN-TDP-43 CRTL and STRESSED vs. MN_healthy CTRL ****$p < 0.0001$. D-M. Violin plots show relative gene expression of MN_healthy STRESSED and MN_TDP-43 CTRL and STRESSED normalized to MN_healthy CTRL. Results are represented as median and quartile range of three independent experiments. Two-way ANOVA followed by Tukey's multiple comparison test was used as statistical analysis for each gene was studied: *$p < 0.05$, **$p < 0.01$, ***<0.001 and ****$p < 0.0001$.

stressful lifestyle by applying the chronic unpredictable mild stress protocol, a well-established rodent model used to induce depressive- and anxiety-like behaviours[11,12]. Indeed a stressful lifestyle can increase the risk of developing anxiety and/or depression, affecting, among the others, mitochondrial membrane depolarization, increased ROS levels and microglial activation[23–28]. Interestingly, we observed that the chronic unpredicted mild stress protocol influenced the ALS onset in mice, in particular by affecting the body weight gain (in both females and males) and determining early motor defects (in females). It is worth noting that a lower Body Mass Index at the time of diagnosis has been associated with a worse prognosis in ALS[29]. Therefore, detecting a stress-related effect on the body weight at the symptom onset may be relevant in the context of this study.

Moreover, in the female h*SOD1*^{G93A} stressed group, among 39 ALS-related genes, *Col1a1* was significantly up-regulated in both the motor cortex and spinal cord, compared to not stressed transgenic mice (CTRL). Furthermore, *Col1a2* was also up-regulated in motor cortex of female stressed group. Otherwise, we observed a significant up-regulation of *Il6* in the motor cortex of h*SOD1*^{G93A} stressed male mice. *Il6* is a crucial cytokine in CNS, with a largely recognized role in several biological processes, including neuroinflammation[30], while collagen is an important protein which can provide structural stability of the extracellular matrix[31]. Interestingly, increased levels of *Il6*[30,32] and collagen accumulation[33] have been referred in ALS patients. Indeed, in our experiments, the altered expression of *Il6*, *Col1a1* and *Col1a2* could be related to oxidative stress, neuroinflammation, DNA damage, apoptosis, autophagy and fibrosis processed, possibly exacerbated by stress[34–37], with evident effects in ALS-predisposed conditions, especially in females. Sex-based divergence is likely attributable to differences in stress response, particularly in terms of reactivity, resilience and adaptation[38–40]. In fact, our results are consistent with previous works showing higher vulnerability of female mice to stressful conditions compared to males[41].

To specifically investigate the MN involvement, we moved to an in vitro experimental model of MNs widely used in ALS research: the NSC-34 cell line. By introducing slight changes to the available protocols for differentiating NSC-34 in MN-like cells[13,42,43], we standardized a simple method to promote MN maturation in both naïve and h*SOD1*-transfected cells (Fig. S2, Fig. S3, Fig. S4 and Fig. 2), enhancing cell-body clusters, neurite length, neurite branch points and ChAT expression.

In the in vitro stress model, we selected OGD to mimic the in vivo stress effects, specifically targeting key stress-activated molecular pathways and associated cellular outcomes. Indeed, OGD can induce neurotoxicity through ROS accumulation and is associated with mitochondrial impairment, neuroinflammation and neuronal

death[44–47]. These cellular dysfunctions are related both to ALS pathogenesis and chronic stress[8]. Therefore, we consider OGD (combining low-glucose medium with $CoCl_2$) as an appropriate model for mimicking chronic stress[48,49],. Our results highlighted a reduced ability of h*SOD1*^{G93A} NSC34 to endure stress (Fig. 3). In h*SOD1*^{WT} cells, upon stress exposure, the mitochondrial membrane potential slightly decreased, while the expression of hypoxic (HIF1α) and apoptotic (cleaved caspase 3) markers increased, suggesting a physiological stress response[49–54]. In contrast, OGD triggered a significant decrease of h*SOD1*^{G93A} mitochondrial membrane potential, without affecting HIF1α and cleaved caspase 3 protein levels. Elevated levels of cleaved caspase 3 have been previously reported in h*SOD1*^{G93A} NSC-34 cells under basal conditions[55]. These observations are in line with our findings, suggesting that the apoptotic pathways are already activated in mutated cells, even in absence of external stress. Thus, we hypothesize that additional stress exposure cannot further amplify this response that may have already reached a plateau due to the pre-existing disease-related activation of apoptosis.

In light of these findings, we investigated the same set of genes in NSC-34 h*SOD1* MNs, normalizing h*SOD1*^{WT} STRESSED, h*SOD1*^{G93A} CTRL and STRESSED, to h*SOD1*^{WT} CTRL MNs (Fig. 4). Then, to better discriminate the mutation- or stress-related effects on gene expression, the significantly deregulated genes were further analysed independently, for both CTRL (i.e. not stressed) and STRESSED groups. The gene expression of mutated MNs has been normalized to WT MNs showing several genes significantly deregulated in CTRL condition (*Cldn5* down-regulated; *Bdnf*, *Casp1*, *Col4a1*, *Fgfr1*, *Gsk3b*, *Hdac7*, *Igf1*, *Il6*, *Nanog* and *Tgfb1* up-regulated). Similarly, the expression of some genes was remarkably affected in h*SOD1*^{G93A} cells compared to h*SOD1*^{WT} upon stress exposure (*Ang*, *Cldn5*, *Gsk3b*, *Hdac7*, *Hspb1*, *Il6* down-regulated; *Casp1*, *Col4a2*, *Igf1* and *Tgfb1* up-regulated). Therefore, stress interferes with some specific intracellular mechanisms, also affecting the predicted PPIs (Fig. 4).

Interestingly, the involvement of certain genes (*Gsk3b*, *Il6*, *Igf1*, together with collagen) seems to be more crucial than others and, based on the GO and pathway enrichment analyses, converges to the key role of PI3K/Akt pathway in the response to stress (Fig. 5). Notably, although PI3K/Akt pathway appeared to be implicated in both experimental conditions, the expression of certain genes (as *Gsk3b* and *Il6*) was different between CTRL and STRESSED groups, highlighting stress-dependent differential regulatory mechanisms in ALS-predisposed conditions. The up-regulation of *Gsk3b* found in the CTRL mutated group aligns with well-known mechanisms of neurodegenerative diseases, including ALS[56–58], in which the Akt inhibition, leading to apoptotic processes and determining caspase 3 protein level increment, may support our results observed in Fig. 3. On the contrary, the down-regulation of *Gsk3b* observed in the STRESSED mutated group can reflect Akt activation, potentially counteracting the apoptotic processes.

Concerning *Il6*, it is known to trigger neuroinflammation in ALS and, although it is a cytokine mainly produced by immune cells, also neurons can express it[30,32,59]: in our experiments, stress apparently modifies its expression, potentially representing an additional protective response.

On the other hand, high levels of *Igf1* can be correlated with a better prognosis of ALS[60], by exerting neuroprotective effects. Based on our results, their levels are strongly reduced upon stress exposure, potentially indicating neuronal distress.

Overall, these findings suggest that in the h*SOD1*^{G93A} MNs stress can trigger different pathways that on one hand could be detrimental, and on the other might represent protective endogenous mechanisms (likely insufficient to halt disease progression, as evidenced by persistently elevated caspase expression).

Pathway enrichment analysis revealed another interesting result concerning the specific pathway activated only in STRESSED experimental condition, i.e. the focal adhesion pathway, with the involvement of *Gsk3b*, *Igf1*, and *Col4a2* (Fig. 5). Notably, focal adhesion, often by the mediation of *Gsk3b* and *Igf1*, regulates oxidative stress induced by chronic stress, depressive symptoms, diet, and general lifestyle factors[61–66].

Moreover, collagen gene family has been previously characterized in brain regions of male mice underwent chronic agonistic interactions[67], supporting our in vivo results for which *COL* genes could be key players of stress regulatory mechanisms in ALS-predisposed conditions.

Interestingly, the results obtained from h*SOD1*^{G93A} NSC-34 cells were consistent with those from hiPCS-derived MNs (Fig. 6), despite the different mutated gene (i.e., *TARDBP*). The morphological parameters of healthy cells (healthy line) indicated a physiological stress response affecting the neurite length and branch point number[68–71]. Moreover, compared to healthy cells, the mutated ones showed significant morphological alterations already in CTRL conditions, that were not further worsened by OGD stress. However, OGD induced significant transcriptional changes in human mutated MNs. Interestingly, gene expression in hiPCS-derived MNs aligned with the results observed in NSC-34 h*SOD1* cell experiments. For instance, *Gsk3b* was down-regulated, and *Col4a2* was up-regulated in STRESSED condition.

In conclusion, our in vivo results (although representing a pilot study, intended to lay the groundwork for our working hypothesis) highlight evident negative effects of stress on the ALS onset/progression. Future investigations at later symptomatic stages and with increased sample size could provide further insights into the impact of stress on disease progression in vivo. Moreover, the in vitro experiments on MNs suggest a crucial role of the PI3K/Akt pathway (triggered by *Gsk3b*, *Il6*, *Igf1* and collagen) in mediating stress response in different ALS-predisposed conditions. The investigation of Gsk3b/GSK3B phosphorylation and the consequent signalling cascade in both PI3K/Akt and focal adhesion pathways could clarify its role in the modulation of Igf1/IGF1, Il6/IL6, and Col/COL proteins. Of course, the absence of protein-level validation and rescue experiments represents a limitation of this study. However, the transcriptomic convergence observed across the used experimental models provides a solid basis for the identification of stress-responsive molecular pathways in ALS-predisposed conditions. Future work will be necessary to validate key candidate genes at the protein level and to functionally assess their contribution to the disease-related phenotype.

Therefore, although further investigations are needed to support our hypothesis, this study enhances our comprehension of the stress role in the ALS-related neurodegenerative mechanisms, paving the way for novel therapeutic targets and encouraging different lifestyle habits.

Methods

Animal care and use

The experimental in vivo procedures were performed in strict accordance with institutional guidelines in compliance with national (D.L. N.26, 04/03/2014) and international law and policies (new directive 2010/63/EU). The study was approved by the Italian Ministry of Health (permit n. 17/2010-B, 30 June 2010, and protocol n. 391/2021-PR). Additionally, an ad hoc Ethical Committee of the University of Turin approved this study. The study is reported in accordance with ARRIVE guidelines. Mice were maintained in the cages, under standard conditions with 12/12-h light/dark cycle and free access to food and water.

Male and female B6SJL-Tg (*SOD1**G93A)1Gur/J mice (The Jackson Laboratory; Bar Harbor, Maine, USA; ref 002726) were used to evaluate in vivo the stress effects. These are transgenic animals expressing a human *SOD1* (h*SOD1*) containing the Gly93Ala mutation, which determines a progressive upper and lower MN loss. The colony was maintained by breeding hemizygous carrier males and B6SJLF1/J females. The offspring genotype was identified by DNA extracted from the mouse tail in order to identify the presence of the h*SOD1* transgene. Forward (oIMR0113; 5' – CAT CAG CCC TAA TCC ATC TGA – 3') and reverse primers (oIMR0114; 3' – CGC GAC TAA CAA TCA AAG TGA – 5') were used, following the Jackson Laboratory instructions and Taq DNA polymerase (GoTaq Flexi DNA Polymerase; Promega; Madison, Wisconsin, USA; ref 9PIM829) protocols for the polymerase chain reaction (PCR).

Overall, 6 transgenic females and 6 transgenic males were used for the experiments: 3 per group were housed in standard conditions (12 h darkness/12 h light), while the others underwent a chronic unpredicted mild stress protocol according to Kumar et al.[11,12], starting at postnatal day 60 (P60). Briefly, the overall duration of the protocol was 28 days, during which cage shaking, cage tilt, cold and warm swim, food/water deprivation, tail pinch, moist bedding, overnight illumination, and a reverse day-night cycle were repeated at least three, non-consecutive times[11,12].

At P90, mice were euthanized by cervical dislocation in order to collect lumbar spinal cord and motor cortex from all the experimental groups.

Rotarod test and weight assessment

Rotarod test was performed to detect motor dysfunctions of the transgenic mice, either housed in standard conditions (CTRL) or stressed. The test was performed from P45 to P89, twice a week, using a 7650-accelerating model of a rotarod apparatus (Ugo Basile, Italy). The first two weeks were considered training sessions. Each test was repeated for three trials, with an accelerated speed from 5 to 32 rpm, and an arbitrary cut-off time of 300 s. The average of three trials was considered. In addition, the mouse weight was assessed after each rotarod session. The values at P89 (end point) were normalized to that at P60 (starting point).

NSC-34 cell cultures

The murine MN-like cell lines, NSC-34 naïve, h*SOD1*^{WT} and h*SOD1*^{G93A} were kindly provided by Prof. Mariotti's laboratory (University of Verona, Italy). h*SOD1*^{WT} and h*SOD1*^{G93A} cells were stably transfected with the human wild type *SOD1* gene or with the mutated one, in previous works[72,73]. The human gene activation is regulated by a doxycycline inducible promoter: 5 µg/ml of doxycycline (Merck, Sigma-Aldrich; St. Louis, MO, USA; ref D9891) for 24 h were used to obtained the human gene expression. Cells were grown in standard experimental condition using DMEM (Merck, Sigma-Aldrich; ref D5796) supplemented with 10% of heat-inactivated fetal bovine serum (FBS; Merck, Sigma-Aldrich; ref F7524), 100 U/ml penicillin and 100 µg/ml streptomycin (Merck, Sigma-Aldrich; ref P4333). Cell differentiation was induced reducing FBS concentration (from 10 to 1%) and adding 20 µM of RA (Merck, Sigma-Aldrich; ref R2625) for 4 days of culture. The culture medium was changed every two days for both standard and differentiation culture conditions.

The OGD stress was induced at DIV (days in vitro) 4 for 24 h using DMEM low glucose (Merck, Sigma-Aldrich; ref D5921), supplemented with 100 µM of $CoCl_2$ (Merck, Sigma-Aldrich; ref 232696). Cells, both under standard and stress conditions, were incubated at 37 °C in 5% CO2.

Human iPSC-derived MN cell cultures

Human MN progenitors were obtained using two lines of human iPSCs, one derived from a healthy patient (56c2) and the other one derived from an ALS patient with the human *TARDBP*^{G298S} mutation, following a standardized protocol[74,75], that has been patented and licensed to Stem Cell Technology (Patent PCT/IB2020/000972). Briefly, the cells were differentiated in embryonic bodies that were dissociated at day 10. The resulting MN progenitor cells were stored into biobanks of I-Stem (Corbeil-Essonnes, France) and Institut Imagine (Paris, France). For the stress experiment, those MN progenitors were seeded in 6 well plates coated with poly-L-ornithine solution (Merck, Sigma-Aldrich; ref P4957) before laminin (Thermo Fisher, Gibco; Waltham, Massachusetts; ref USA23017015), at ~ 1×10^5 cells/cm^2 of density. The progenitors were seeded and further differentiated intro mature MNs for 14 days in medium consisting to DMEM-F12 Glutamax/Neurobasal (Thermo Fisher, Gibco; ref 10565018/21103049; 1:1 ratio), N2 supplement/B27 no vitamin A supplement (Thermo Fisher, Gibco; ref 17502048/A3353501; 1:2 ratio), 0.1% of β-mercaptoethanol (Thermo Fisher, Gibco; ref 31350010) and 0.1% of Pen Strep (Thermo Fisher, Gibco; ref 15140122), supplemented with 100 nM of retinoic acid (Merck, Sigma-Aldrich; ref R2625), 0.5 µM of Smoothened Agonis (SAG; STEMCELLS Technologies; Vancouver, British Columbia, Canada; ref 73414;), 1 µM of Brain-Derived Neurotrophic Factor (*BDNF*; PreproTech; Rocky Hill, New Jersey, USA; ref 17874463), 1 µM of Glial-Derived Neurotrophic Factor (GDNF; PreproTech; ref 17814073),

10 nM of γ-secretase inhibitor (DAPT, STEMCELLS Technologies; ref 72792) and 10 μM of Y-27,632 (ROCK Inhibitor; STEMCELLS Technologies; ref 72307). Y-27,632 was eliminated the day after seeding at by medium refreshing and medium was refreshed every three days. The OGD stress was induced at day 24 using DMEM low glucose, supplemented with 100 μM of $CoCl_2$ (Merck, Sigma-Aldrich; ref 232696). Cells were incubated at 37 °C in 5% CO_2 during the entire period of the experiments.

Cell viability assay

3-[4,5-dimethylthiazol-2-yl]-2,5 diphenyl tetrazolium bromide) assay (MTT assay) for RA and $CoCl_2$ treatments on NSC-34 cells was performed using cell proliferation kit I (MTT) (Merck, Roche; Basel, Switzerland; ref 11465007001) following the manufacture's instruction. Cells were plated in 96-wells plates (3×10^3 cells/well) and maintained in standard growth culture conditions for 24 h before testing different concentrations of RA (1 μM, 5 μM, 10 μM, 15 μM and 20 μM) for 2, 4, 6 and 8 days, with and without doxycycline treatment. In order to perform $CoCl_2$ MTT, cells were also seeded in 96-wells plates (3×10^3 cells/well) and were kept in standard growth culture for 24 h. Cells were differentiated for 4 days: then, DMEM low glucose supplemented with doxycycline and different concentrations of $CoCl_2$ (50 μM, 100 μM, 200 μM, 300 μM and 400 μM) were tested for 24 h. The absorbance was measured at 550 nm using a microplate reader (Tecan Infinite M nano) in at least two wells per condition, replicating three independent experiments.

Neurotrack analysis

Incucyte Neurotrack software module was used to validate MN differentiation of NSC-34 naïve, h*SOD1*^{WT} and h*SOD1*^{G93A} cells, evaluating cell-body cluster, neurite length and neurite branch point. The same morphological parameters were measured for analysing the stress impact on human MNs (hMNs). NSC-34 cells were seeded in 96-well plates at the density of 1.5×10^4 cells/cm^2 for four experimental conditions: standard medium with 1% fetal bovine serum (FBS), with and without doxycycline, and differentiated condition (standard medium with 1% serum, supplemented with 20 μM of RA), with and without doxycycline. Instead, hMNs (both healthy and TDP-43 mutated cells) were plated in 6-well plates at 1×10^5 cells/cm^2 for two experimental conditions: control and stressed conditions. Five and two wells per conditions of NSC-34 cells and hMNs, respectively, were analysed using three independent experiments [each performed at different passages (p) of the same NSC-34 cell line, specifically between p18 and p24], after the acquisition by the built-in Basler Ace 1920 –155 μm camera of the Incucyte system (Sartorius; Göttingen, Germany). NSC-34 segmentation mode related to cell-body cluster was set up in brightness considering 1 as range of segmentation adjustment. Clean-up was regulated for min cell width, set to 7 μm, while cell-body cluster filters were not applied. Filtering related to neurite parameters was configured as better setting 0.3 for neurite sensitivity and 1 μm for neurite width. For hMNs, filtering of neurite parameters was configured ad best, while the neurite sensitivity and the neurite width were set-up to 0.35 and 2, respectively.

Immunofluorescence

To analyse cell differentiation in vitro, murine cells were seeded in 24 wells plates onto poly-D-lysine (Merck, Sigma-Aldrich; ref A-003-E) coated-coverslips at the density of 1.5×10^4 cells/cm^2 under four experimental conditions: standard medium 1% serum, with and without doxycycline, and differentiated condition, with and without doxycycline. Cells were fixed in 4% paraformaldehyde for 10 min at DIV5. Cell permeabilization was performed in PBS-0.2% Triton-X100, while blocking of unspecific sites was done in PBS-0.1% Triton-X100 and 5% Normal Donkey Serum (NDS; Merck, Sigma-Aldrich; ref. D9663). As primary antibody, we used rabbit Anti-Choline Acetyltransferase (ChAT) (Merck, Sigma-Aldrich; ref Ab143; 1:200), incubated in PBS-0.1% Triton-X100 and 5% NDS. As secondary antibody, we used Cy3 AffiniPure Donkey Anti-Rabbit IgG (H + L) (Jackson ImmunoResearch; West Grove, Pennsylvania, USA; ref 711-165-152; 1:200) incubated in PBS and 2% NDS. Coverslips were mounted on microscope slides using mounting medium Mowiol/Dabco and the image acquisitions were realized by Eclipse E600 (Microfire Camera 2-Megapixel Color Imaging, 1600 × 1200). Images were thresholded identically across all experimental conditions and CTCF was analysed for at least ten cells from three independent experiments using ImageJ software.

Mitochondrial imaging

Mitochondrial membrane potential was evaluated using MitoTracker Red CMXRos (Thermo Fisher; ref M7512), a mitochondrial dye based on X-rosamine derivate. The probe was added to the medium of NSC-34 h*SOD1*^{WT} and h*SOD1*^{G93A} cells under two experimental conditions: control and stressed conditions. The final concentration of the probe was 100 nM and was maintained for 25 min, keeping the cell plates in the incubator at 37 °C in 5% CO_2. Then, medium was changed and the image acquisitions were performed by the built-in Basler Ace 1920 –155 μm camera of the Incucyte system. "Cell-by-cell" software module was used in order to obtain the Total Orange Object Integrated Intensity normalized to Phase Object Count. All the analysis parameters were configured following Sartorius recommendations.

Western blot

Western blot was performed in order to verify the stress impact on NSC-34 h*SOD1*^{WT} and h*SOD1*^{G93A} cells. Proteins were extracted using a lysis buffer consisting of RIPA buffer (Merck, Millipore; Darmstadt, Germany; ref 20–188) supplemented with cOmplete Protein Inhibitor Cocktail [1X] (Merck, Roche; ref 11697498001), sodium orthovanadate [2 mM] (Merck, Sigma-Aldrich; ref S6508), Phenylmethanesulfonyl fluoride [1 mM] (Thermo Fisher; ref 36978) and dithiothreitol [1 mM] (Thermo Fisher; ref R0861). Lysates were sonicated for 8 min using Ultrasonic baths Bandelin Sonorex at room temperature and centrifuged at 3×10^3 rpm for 10 min at 4 °C. Protein quantifications were performed following manufacturer's instructions of Bio-Rad Protein Assay

Dye Reagent Concentrate (Bio-Rad Laboratories; Hercules, California, USA; ref 5000006). 25 µg of proteins were mixed to NuPAGE LDS Sample Buffer [1X] (Thermo Fisher; ref NP0007) and NuPAGE Sample Reducing Agent [1X] (Thermo Fisher, Invistrogen; ref NP0004), denatured for 5 min at 95 °C, separated using 4–20% Mini-PROTEAN TGX Precast Protein Gels (Bio-Rad Laboratories; ref 4561094;) and transferred into nitrocellulose membrane using Trans-Blot Turbo RTA Mini 0.2 µm Nitrocellulose Transfer Kit (Bio-Rad Laboratories; ref 1704270). Blots were blocked with EveryBlot Blocking Buffer (Bio-Rad Laboratories; ref 12010020) and incubated overnight with selected primary antibodies: mouse anti HIF1α (Santa Cruz; Dallas, Texas, USA; ref 28b; sc-13515; 1:500), rabbit anti Cleaved Caspase-3 (Cell signalling; Danvers, Massachusetts, USA; ref Asp 175; 9661; 1:500) and mouse anti β-Tubulin (Merck, Sigma-Aldrich; ref T8328; 1:1,000). Subsequently, membranes were incubated for 1 h with appropriate secondary antibodies: Goat Anti-Mouse IgG (H + L)-HRP Conjugate (Bio-Rad Laboratories; ref 1706516; 1: 10,000) and Goat Anti-Rabbit IgG (H + L)-HRP Conjugate (Bio-Rad Laboratories; ref 1706515; 1:10,000). The bands were exposed to Clarity Max Western ECL Substrate (Bio-Rad Laboratories; ref 1705062) and their signals were detected using ChemiDoc imaging system (Bio-Rad Laboratories; USA). Densitometric analysis of the bands was performed using Bio-Rad Laboratories Image Lab software and target values were normalized to β-Tubulin signal.

Quantitative reverse transcription polymerase chain reaction (RT-qPCR)

Total RNA extraction from murine tissues and NSC-34 cell lines was performed using Maxwell RSC simply RNA Cells Kit (Promega; ref AS1390), while for hMNs the RNeasy plus mini kit was used (QIAGEN; Venlo, Netherlands; ref 74134). RNA concentrations were quantified using Nano Quant Plate available for microplate reader Tecan Infinite M nano (Tecan, Switzerland) and iScript Advanced cDNA Synthesis Kit (Bio-Rad Laboratories; ref 1725038) was used for RNA to cDNA retrotranscription. For qPCR, species-specific (mouse or human) Prime PCR Disease State Panels (Bio-Rad Laboratories; ref 10036315 or 10034810) were used, based on SYBR detection workflows (iTaq Universal SYBR Green Supermix; Bio-Rad Laboratories; ref 1725124) and predesigned for ALS-related genes (Table S1). cDNA concentration was calibrated for each experimental model: charged-quantity of cDNA for mouse tissues and human MNs was 25 ng/µl, while for NSC-34 cell lines was 75 ng/µl. The results were analysed following $2^{-\Delta\Delta Ct}$ method considering *Gapdh* gene as housekeeping. Heatmaps, violin blots and bar plots were used to represent gene expression analyses.

Protein-protein interaction (PPI) data

Protein-protein interaction (PPI) related to deregulated genes in h*SOD1*^{G93A} NSC-34 cells compared to h*SOD1*^{WT} ones was analysed in separated analysis for control and stressed experimental condition using The Search Tool for the Retrieval of Interacting Genes (STRING) database (free online platform: https://string-db.org, accessed on 8 May 2024 and 19 March 2024, respectively).

GO and pathway enrichment analyses

GO and pathway enrichment analyses were performed on genes significantly deregulated in h*SOD1*^{G93A} NSC-34 cells compared to h*SOD1*^{WT} ones. Separated analyses were applied for control and stressed experimental condition using SRplot (free online platform: http://www.bioinformatics.com.cn/SRplot, accessed on 8 May 2024 and 15 March 2024, respectively). GO three ontology plots were used to show biological processes (BP), cellular component (CC) and molecular function (MF), highlighting enrichment score in the x-axis of the graph. Instead, pathway enrichment analysis was visualized through cnet plots to facilitate the interpretation of gene interactions and their involvement in a specific pathway (or category), by using log2 fold change about the gene expression and bubble size for the gene's numbers implicated in a specific category.

Statistical analysis

Data are shown as media ± SD and/or as median and quartile range of at least three independent experiments. Statistical analyses were conducted using two-way ANOVA (followed by Dunnett or Sidák or Tukey multiple comparison or by Uncorrected Fisher's LDS) or Mixed-effects (followed by Uncorrected Fisher's LDS or Tukey's multiple comparison tests) or Unpaired t-test. These analyses and corresponding graphs (including heatmaps) were performed using GraphPad Prism version 10.1.2 for Windows (GraphPad Software, Boston, Massachusetts USA, www.graphpad.com). Results were considered significant at $P < 0.05$.

Data availability

The details of mouse model are available at https://www.jax.org/strain/002726# and the data regarding primers for their genotyping are here: https://www.jax.org/Protocol? stockNumber=002726&protocolID=29082. Instea d, the data regarding Prime PCR Disease State Panels (Bio-Rad Laboratories) are available at https://commerce.bio-rad.com/en-us/prime-pcr-assays/pathway/amyotrophic-lateral-sclerosis. Finally, STRING analysis and GO with Pathway enrichment analysis are free accesses at https://string-db.org/ and https://www.bioinformatics.com.cn/en, respectively.

Received: 13 February 2025; Accepted: 12 May 2025
Published online: 21 May 2025

References

1. Chia, R., Chiò, A. & Traynor, B. J. Novel genes associated with amyotrophic lateral sclerosis: diagnostic and clinical implications. *Lancet Neurol.* **17**, 94–102 (2018).
2. Mead, R. J., Shan, N., Reiser, H. J., Marshall, F. & Shaw, P. J. Amyotrophic lateral sclerosis: a neurodegenerative disorder poised for successful therapeutic translation. *Nat. Rev. Drug Discov.* **22**, 185–212 (2023).

3. Akçimen, F. et al. Amyotrophic lateral sclerosis: translating genetic discoveries into therapies. *Nat. Rev. Genet.* **24**, 642–658 (2023).
4. Vasta, R., Chia, R., Traynor, B. J. & Chiò, A. Unraveling the complex interplay between genes, environment, and climate in ALS. *eBioMedicine* **75**, 103795 (2022).
5. Mejzini, R. et al. ALS genetics, mechanisms, and therapeutics: Where are we now? *Front. Neurosci*. **13** (2019).
6. Godoy, L. D., Rossignoli, M. T., Delfino-Pereira, P. & Garcia-Cairasco, N. & de Lima Umeoka, E. H. A comprehensive overview on stress neurobiology: Basic concepts and clinical implications. *Front Behav. Neurosci*. **12** (2018).
7. Dallman, M. F. Fast glucocorticoid actions on brain: back to the future. *Front. Neuroendocr.* **26**, 103–108 (2005).
8. Lucassen, P. J. et al. Neuropathology of stress. *Acta Neuropathol.* **127**, 109–135 (2014).
9. Madore, C., Yin, Z., Leibowitz, J., Butovsky, O. & Microglia, lifestyle stress, and neurodegeneration. *Immunity* **52**, 222–240 (2020).
10. Peña-Bautista, C., Casas-Fernández, E., Vento, M., Baquero, M. & Cháfer-Pericás, C. Stress and neurodegeneration. *Clin. Chim. Acta*. **503**, 163–168 (2020).
11. Kumar, B., Kuhad, A. & Chopra, K. Neuropsychopharmacological effect of Sesamol in unpredictable chronic mild stress model of depression: behavioral and biochemical evidences. *Psychopharmacology* **214**, 819–828 (2011).
12. Molina, V. A. et al. Effect of chronic variable stress on monoamine receptors: influence of Imipramine administration. *Pharmacol. Biochem. Behav.* **35**, 335–340 (1990).
13. Maier, O. et al. Differentiated NSC-34 motoneuron-like cells as experimental model for cholinergic neurodegeneration. *Neurochem. Int.* **62**, 1029–1038 (2013).
14. Farhud, D. D. Impact of lifestyle on health. *Iran. J. Public. Health*. **44**, 1442–1444 (2015).
15. Gaur, A. et al. Sleep. Alzheimer: Link. *Mædica* **17**, 177 (2022).
16. Pacholko, A. G., Wotton, C. A. & Bekar, L. K. Poor diet, stress, and inactivity converge to form a 'perfect storm' that drives Alzheimer's disease pathogenesis. *Neurodegener Dis.* **19**, 60–77 (2019).
17. Palpatzis, E. et al. Lifetime stressful events associated with Alzheimer's pathologies, neuroinflammation and brain structure in a risk enriched cohort. *Ann. Neurol.* **95**, 1058–1068 (2024).
18. Dallé, E. & Mabandla, M. V. Early life stress, depression and Parkinson's disease: A new approach. *Mol. Brain*. **11**, 18 (2018).
19. Vlajinac, H. et al. The stressful life events and Parkinson's disease: a case-control study. *Stress Health*. **29**, 50–55 (2013).
20. Bonanni, L. et al. Post traumatic stress disorder heralding the onset of semantic frontotemporal dementia. *J. Alzheimers Dis.* **63**, 203–215 (2018).
21. Kullmann, J. A. P., Hayes, S. & Pamphlett, R. Is psychological stress a predisposing factor for amyotrophic lateral sclerosis (ALS)? An online international case-control study of premorbid life events, occupational stress, resilience and anxiety. *PLOS ONE*. **13**, e0204424 (2018).
22. Okamoto, K. et al. Lifestyle factors and risk of amyotrophic lateral sclerosis: a case-control study in Japan. *Ann. Epidemiol.* **19**, 359–364 (2009).
23. Warren, A., Nyavor, Y., Beguelin, A. & Frame, L. A. Dangers of the chronic stress response in the context of the microbiota-gut-immune-brain axis and mental health: A narrative review. *Front. Immunol*. **15** (2024).
24. Gomes, R., Santos, C., Descalço, N. & Moutinho, F. Does my lifestyle explain my depression? The role of exercise, diet and smoking in the prevention of depression. *Eur. Psychiatry*. **65**, S680–S681 (2022).
25. Firth, J. et al. A meta-review of lifestyle psychiatry: the role of exercise, smoking, diet and sleep in the prevention and treatment of mental disorders. *World Psychiatry*. **19**, 360–380 (2020).
26. Visentin, A. P. V. et al. Targeting inflammatory-mitochondrial response in major depression: Current evidence and further challenges. *Oxid. Med. Cell. Longev.* 2972968 (2020).
27. Purba, A. & Demou, E. The relationship between organisational stressors and mental wellbeing within Police officers: a systematic review. *BMC Public. Health*. **19**, 1286 (2019).
28. Wang, Y. L. et al. Microglial activation mediates chronic mild stress-induced depressive- and anxiety-like behavior in adult rats. *J. Neuroinflamm.* **15**, 21 (2018).
29. Wang, M. D., Little, J., Gomes, J., Cashman, N. R. & Krewski, D. Identification of risk factors associated with onset and progression of amyotrophic lateral sclerosis using systematic review and meta-analysis. *Neurotoxicology* **61**, 101–130 (2017).
30. Erta, M., Quintana, A. & Hidalgo, J. Interleukin-6, a major cytokine in the central nervous system. *Int. J. Biol. Sci.* **8**, 1254–1266 (2012).
31. Soles, A. et al. Extracellular matrix regulation in physiology and in brain disease. *Int. J. Mol. Sci.* **24**, 7049 (2023).
32. Pronto-Laborinho, A. et al. Interleukin-6 and amyotrophic lateral sclerosis. *J. Neurol. Sci.* **398**, 50–53 (2019).
33. Garbuzova-Davis, S. et al. Impaired blood–brain/spinal cord barrier in ALS patients. *Brain Res.* **1469**, 114–128 (2012).
34. Boin, F. et al. Oxidative stress-dependent activation of collagen synthesis is induced in human pulmonary smooth muscle cells by Sera from patients with scleroderma-associated pulmonary hypertension. *Orphanet J. Rare Dis.* **9**, 123 (2014).
35. Fu, X. H. et al. COL1A1 affects apoptosis by regulating oxidative stress and autophagy in bovine cumulus cells. *Theriogenology* **139**, 81–89 (2019).
36. Martins, S. G., Zilhão, R., Thorsteinsdóttir, S. & Carlos, A. R. Linking oxidative stress and DNA damage to changes in the expression of extracellular matrix components. *Front. Genet.* **12** (2021).
37. Zhuang, L. et al. RNA COL1A2 mediates high Glucose-Induced oxidative stress and pyroptosis by regulating MiR-424-5p/SGK1 in diabetic nephropathy. *Appl. Biochem. Biotechnol.* **195**, 7652–7667 (2023).
38. Goldfarb, E. V., Seo, D. & Sinha, R. Sex differences in neural stress responses and correlation with subjective stress and stress regulation. *Neurobiol. Stress*. **11**, 100177 (2019).
39. Verma, R., Balhara, Y. P. S. & Gupta, C. S. Gender differences in stress response: role of developmental and biological determinants. *Industrial Psychiatry J.* **20**, 4 (2011).
40. Zhang, A. Y., Elias, E. & Manners, M. T. Sex-dependent astrocyte reactivity: unveiling chronic stress-induced morphological changes across multiple brain regions. *Neurobiol. Dis.* **200**, 106610 (2024).
41. Dalla, C. et al. Chronic mild stress impact: are females more vulnerable? *Neuroscience* **135**, 703–714 (2005).
42. Madji Hounoum, B. et al. NSC-34 motor neuron-like cells are unsuitable as experimental model for glutamate-mediated excitotoxicity. *Front Cell. Neurosci* **10** (2016).
43. Nango, H. et al. Highly efficient conversion of motor neuron-like NSC-34 cells into functional motor neurons by prostaglandin E2. *Cells* **9**, 1741 (2020).
44. Almeida, A., Delgado-Esteban, M., Bolaños, J. P. & Medina, J. M. Oxygen and glucose deprivation induces mitochondrial dysfunction and oxidative stress in neurones but not in astrocytes in primary culture. *J. Neurochem.* **81**, 207–217 (2002).
45. Chiang, M. C. et al. Resveratrol mitigates oxygen and glucose Deprivation-Induced inflammation, NLRP3 inflammasome, and oxidative stress in 3D neuronal culture. *Int. J. Mol. Sci.* **23**, 11678 (2022).
46. Gouix, E. et al. Oxygen glucose deprivation-induced astrocyte dysfunction provokes neuronal death through oxidative stress. *Pharmacol. Res.* **87**, 8–17 (2014).
47. Shi, L. et al. Sirt1 regulates oxidative stress in oxygen-glucose deprived hippocampal neurons. *Front. Pediatr*. **8** (2020).
48. Guo, M. et al. Hypoxia-mimetic agents desferrioxamine and Cobalt chloride induce leukemic cell apoptosis through different hypoxia-inducible factor-1alpha independent mechanisms. *Apoptosis* **11**, 67–77 (2006).
49. Xu, R. et al. Linking hypoxic and oxidative insults to cell death mechanisms in models of ALS. *Brain Res.* **1372**, 133–144 (2011).
50. Chavez, J. C. & LaManna, J. C. Activation of Hypoxia-Inducible Factor-1 in the rat cerebral cortex after transient global ischemia: potential role of Insulin-Like growth Factor-1. *J. Neurosci.* **22**, 8922–8931 (2002).

51. Han, A. R., Yang, J. W., Na, J. M., Choi, S. Y. & Cho, S. W. Protective effects of N,4,5-trimethylthiazol-2-amine hydrochloride on hypoxia-induced β-amyloid production in SH-SY5Y cells. *BMB Rep.* **52**, 439–444 (2019).
52. Newcomb-Fernandez, J. K. et al. Concurrent assessment of Calpain and caspase-3 activation after oxygen-glucose deprivation in primary septo-hippocampal cultures. *J. Cereb. Blood Flow. Metab.* **21**, 1281–1294 (2001).
53. Toriuchi, K. et al. Prolonged astrocyte-derived erythropoietin expression attenuates neuronal damage under hypothermic conditions. *J. Neuroinflammation*. **17**, 141 (2020).
54. Zeiger, S. L. H. et al. Neuron specific metabolic adaptations following multi-day exposures to oxygen glucose deprivation. *Biochim. Et Biophys. Acta (BBA) - Mol. Basis Disease*. **1802**, 1095–1104 (2010).
55. Sathasivam, S., Grierson, A. J. & Shaw, P. J. Characterization of the caspase cascade in a cell culture model of SOD1-related Familial amyotrophic lateral sclerosis: expression, activation and therapeutic effects of Inhibition. *Neuropathol. Appl. Neurobiol.* **31**, 467–485 (2005).
56. Choi, H. J., Cha, S. J., Lee, J. W., Kim, H. J. & Kim, K. Recent advances on the role of GSK3β in the pathogenesis of amyotrophic lateral sclerosis. *Brain Sci.* **10**, 675 (2020).
57. Long, H. Z. et al. PI3K/AKT signal pathway: A target of natural products in the prevention and treatment of Alzheimer's disease and Parkinson's disease. *Front. Pharmacol.* **12** (2021).
58. Romorini, L. et al. AKT/GSK3β signaling pathway is critically involved in human pluripotent stem cell survival. *Sci. Rep.* **6**, 35660 (2016).
59. Chen, Y., Xia, K., Chen, L. & Fan, D. Increased interleukin-6 levels in the astrocyte-derived exosomes of sporadic amyotrophic lateral sclerosis patients. *Front. Neurosci.* **13** (2019).
60. Nagel, G. et al. Association of Insulin-like growth factor 1 concentrations with risk for and prognosis of amyotrophic lateral Sclerosis – Results from the ALS registry Swabia. *Sci. Rep.* **10**, 736 (2020).
61. Guo, N. et al. PI3K/AKT signaling pathway: molecular mechanisms and therapeutic potential in depression. *Pharmacol. Res.* **206**, 107300 (2024).
62. Kitagishi, Y., Nakanishi, A., Ogura, Y. & Matsuda, S. Dietary regulation of PI3K/AKT/GSK-3β pathway in Alzheimer's disease. *Alzheimer's Res. Therapy*. **6**, 35 (2014).
63. Kitagishi, Y. et al. Certain diet and lifestyle May contribute to islet β-cells protection in Type-2 diabetes via the modulation of cellular PI3K/AKT pathway. *Open. Biochem. J.* **8**, 74–82 (2014).
64. Kuang, W. H., Dong, Z. Q., Tian, L. T. & Li, J. IGF-1 defends against chronic-stress induced depression in rat models of chronic unpredictable mild stress through the PI3K/Akt/FoxO3a pathway. *Kaohsiung J. Med. Sci.* **34**, 370–376 (2018).
65. Liu, C. et al. IGF-1 via PI3K/Akt/S6K signaling pathway protects DRG neurons with high Glucose-induced toxicity. *Open. Life Sci.* **14**, 502 (2019).
66. Zhang, Z. Q. et al. Chronic stress promotes glioma cell proliferation via the PI3K/Akt signaling pathway. *Oncol. Rep.* **46**, 202 (2021).
67. Smagin, D. A., Galyamina, A. G., Kovalenko, I. L., Babenko, V. N. & Kudryavtseva, N. N. Aberrant expression of collagen gene family in the brain regions of male mice with behavioral psychopathologies induced by chronic agonistic interactions. *BioMed. Res. Int.* 7276389 (2019).
68. Dhawan, S. et al. Reactive oxygen species mediate activity-regulated dendritic plasticity through NADPH oxidase and aquaporin regulation. *Front. Cell. Neurosci.* **15** (2021).
69. Dioli, C. et al. Chronic stress triggers divergent dendritic alterations in immature neurons of the adult hippocampus, depending on their ultimate terminal fields. *Transl. Psychiatry*. **9**, 143 (2019).
70. Shields, S., Wilkes, O., Gozes, I. & Sanchez-Soriano, N. Oxidative stress promotes axonal atrophy through alterations in microtubules and EB1 function. 07.12.603221. Preprint https://doi.org/10.1101/2024.07.12.603221 (2024).
71. Ustyantseva, E. et al. Oxidative stress monitoring in iPSC-derived motor neurons using genetically encoded biosensors of H2O2. *Sci. Rep.* **12**, 8928 (2022).
72. Bonafede, R. et al. Exosome derived from murine adipose-derived stromal cells: neuroprotective effect on in vitro model of amyotrophic lateral sclerosis. *Exp. Cell. Res.* **340**, 150–158 (2016).
73. Calabria, E. et al. ASCs-Exosomes recover coupling efficiency and mitochondrial membrane potential in an in vitro model of ALS. *Front. Neurosci.* **13**, 1070 (2019).
74. Maury, Y. et al. Combinatorial analysis of developmental cues efficiently converts human pluripotent stem cells into multiple neuronal subtypes. *Nat. Biotechnol.* **33**, 89–96 (2015).
75. De Lamotte, J. D. et al. Optogenetically controlled human functional motor endplate for testing botulinum neurotoxins. *Stem Cell. Res. Ther.* **12**, 599 (2021).

Acknowledgements

The authors would like to thank Prof. Raffaella Mariotti and her group (University of Verona, Italy) for kindly providing the NCS-34 naïve, hSOD1WT and hSOD1G93A cell lines. Moreover, the authors acknowledge the support of Dr. Sandrine Baghdoyan (I-STEM, INSERM, Evry, France) with the bioinformatic analyses. D.M.R.'s research has been conducted during and with the support of the Italian national inter-university PhD course in Sustainable Development and Climate Change (link: www.phd-sdc.it). This work was supported by the Italian Ministry of University and Research (MUR) national project "Dipartimenti di Eccellenza 2023-2027", awarded to the Department of Neuroscience "Rita Levi Montalcini" (University of Turin).

Author contributions

MB and DMR conceived and designed the study. DMR, IS, NB, EP and SC performed the experimental procedures. DMR analysed the experimental results. MB, DMR, NB, EK and CM interpreted the data. MB and DMR wrote the draft. All authors reviewed the manuscript.

Declarations

Competing interests

The authors declare no competing interests.

Additional information

Supplementary Information The online version contains supplementary material available at https://doi.org/10.1038/s41598-025-02167-9.

Correspondence and requests for materials should be addressed to M.B.